LBL-11522 c.2
Preprint

Lawrence Berkeley Laboratory
UNIVERSITY OF CALIFORNIA

Submitted to Nuclear Physics

MICROSCOPIC CALCULATIONS OF FISSION BARRIERS AND CRITICAL ANGULAR MOMENTA FOR EXCITED HEAVY NUCLEAR SYSTEMS

Michael Diebel, Klaus Albrecht and Rainer W. Hasse

September 1980

Prepared for the U.S. Department of Energy under Contract W-7405-ENG-48

DISCLAIMER

LBL-Preprint

MICROSCOPIC CALCULATIONS OF FISSION BARRIERS AND CRITICAL ANGULAR MOMENTA FOR EXCITED HEAVY NUCLEAR SYSTEMS†

Michael Diebel[#], Klaus Albrecht[‡] and Rainer W. Hasse[#]

Sektion Physik, Universität München, 8046 Garching, West Germany

Lawrence Berkeley Laboratory
University of California
Berkeley, CA 94720

September 1980

---

†Part of PhD thesis of M.D. Work supported in part by the Bundesministerium für Forschung und Technologie.

#Present address: Institut für Theoretische Physik, Universität Giessen, 6300 Giessen, West Germany.

‡Present address: Department of Physics, University of Transkei, Umtata, Republic of Transkei, South Africa.

#Work partly done at the Nuclear Science Division, Lawrence Berkeley Laboratory, Berkeley, CA 94720, USA, under the auspices of the Division of Nuclear Physics of the Office of High Energy and Nuclear Physics of the U.S. Department of Energy, contract W-7405-ENG-48, and supported by the Deutsche Forschungsgemeinschaft.

Abstract

An extended version of Strutinsky's macro-microscopic method is used to calculate effective potential energies for rotating, excited heavy compound nuclei undergoing fission. Nuclear deformation is parameterized in terms of Lawrence's family of shapes. A two-center single-particle potential corresponding to these shapes is employed, with BCS pairing added. Statistical excitation is introduced by temperature-dependent occupation of (quasi-) particle energy levels. We calculate shell corrections to the energy, the free energy and the entropy as functions of deformation and temperature. The associated average quantities are derived from a temperature-dependent liquid drop model. The resulting static deformation energy is augmented by the rotational energy to yield the isothermal effective potential energy as a function of deformation, temperature and angular momentum. Moments of inertia are obtained from the adiabatic cranking model with temperature-dependent pairing included.

We have also calculated the effective potential for constant entropy rather than constant temperature. Although this isentropic process physically is more appropriate than the isothermal process, it has not been treated before. For the same amount of excitation energy in the spherical state of the compound nucleus, the isentropic barriers turn out higher than the isothermal ones. For both processes we have extracted the critical angular momentum (defined as the one for which the barrier approximately vanishes) as a function of excitation. Our model is applied to the superheavy nuclei $^{270}110$, $^{278}110$, $^{298}114$, $^{292}118$ and $^{322}128$, which have been tried to form in krypton and argon induced heavy ion reactions.

1. Introduction

The increasing availability of heavy ion beams in recent years has stimulated experimental studies of collective motions of very heavy nuclear systems with large amounts of angular momentum that were inaccessible before. The natural first step towards a theoretical description of such systems is to gain a quantitative understanding of the behaviour of a compound nucleus with respect to its shape and rotational degrees of freedom as functions of the excitation energy and the angular momentum.

A detailed knowledge of these properties is required in order to describe e.g. the fission of a rotating heavy nucleus or the fusion versus fission competition in a composite formed by colliding heavy ions. In particular, the chance to reach via a heavy ion reaction the island of relatively stable superheavy nuclei predicted by theory depends critically on how much excitation and angular momentum such nuclei can tolerate before they fission too quickly to be detected.

Whereas the potential energies of deformation for nonrotating cold nuclei have been mapped extensively in a variety of models, much less is known about the rotating, excited nucleus. Only for the case of a classical liquid drop with rigid-body moment of inertia and no excitation, a fairly complete survey has been given by Cohen, Plasil and Swiatecki[1]). It is well known, however, that shell effects play an important role in heavy nuclei and form the very basis for the conjectured existence of superheavy nuclei. Further, we know from low-energy rotational spectra that the nuclear moment of inertia is

considerably smaller (due to pairing) than the rigid-body value. In any realistic description of a rotating nucleus at least these features must be incorporated.

The macro-microscopic method due to Strutinsky[2]) is obviously the next level of sophistication to be considered. This method has been widely and successfully used to calculate deformation energies for nonrotating cold nuclei, see e.g. ref.[3]). It was combined by Jensen and Damgaard[4]) with the statistical model[5]) of excitation, including pairing. On the other hand, Strutinsky's shell correction method has been applied to calculate effective potential energies of rotating cold nuclei by various groups[6-9]) of authors. Mustafa and Kumar[6]) reported on results for ^{240}Pu and ^{298}114, using a two-center shell model with pairing and treating rotation in the adiabatic limit. These effects were accounted for in refs.[7-9]), but here pairing was excluded. Neergård et al.[7]) used a triaxial harmonic oscillator potential without spin-orbit coupling or other corrections to compute equilibrium deformations of rare-earth nuclei as a function of angular momentum. The Lund group[8]) employed the same potential with these corrections included. They obtained maps of the effective potential for a range of rare-earth and lighter nuclei as well as for Z = 114. In a similar way, the Jülich group[9]) investigated the fission instability of a series of nuclei using a deformed Woods-Saxon potential. Both, rotation and excitation, were considered by Ignatyuk et al.[10]), who calculated spherical energies and level densities for heavy nuclei with pairing excluded.

The purpose of this paper is to study rotating hot nuclei by treating (statistical) excitation, rotation and pairing simultaneously. In the next section we state our model and the general physical assumptions made. In sect. 3 we give explicit expressions for the statistical quantities and the moment of inertia. Shell corrections to the former quantities are derived in sect. 4. The corresponding average quantities required in the macro-microscopic approach are taken from a liquid-drop model including excitation for greater consistency. As this constitutes a new element within the Strutinsky method, we discuss the properties of the excited liquid drop in detail in sect. 5. While sects. 3-5 do not refer to a particular parameterization of the nuclear shape or the associated single-particle Hamiltonian, we specify our choice of these in sect. 6. In the last section we present and discuss our numerical results for five superheavy systems and compare them to previous calculations where available.

2 General model assumptions

2.1. DEFORMATION

In the macro-microscopic approach, one uses classical parameters describing the shape and orientation of the nucleus. For computational reasons the number of these parameters must be as small as possible. We assume axial symmetry and reflexion symmetry about the equatorial plane. Nuclear shapes are specified by two deformation parameters (elongation and constriction) covering deformed ground states and symmetric fission shapes. This means we have sacrificed triaxiality, which

is important for (cold) medium-heavy nuclei and which has been treated in refs. [7,8]) in lieu of constriction (necking-in). Judging from refs. [8,11]) we expect, however, that triaxiality is less relevant for the excited superheavy systems considered in this paper. For such systems, also the mass asymmetry degree of freedom neglected here plays a minor role[3,12]). Details of the shape parameterization are given in sect. 6.

2.2 ROTATION

In a nucleus, rotation is a complicated interplay between collective and intrinsic degrees of freedom. The intrinsic states are affected by the collective centrifugal and Coriolis forces. In particular, the latter force acts with opposite signs on the two nucleons in a paired state (Coriolis anti-pairing effect, CAP). The nucleus like any asymmetric top rotates about an axis which, in general, does not coincide with one of its principal axes. The precession or wobbling, cf. ref.[8]), may cause intrinsic excitation.

For simplicity, we neglect intrinsic angular momentum and further assume that the nucleus rotates about the principal axis having the largest moment of inertia, namely the one perpendicular to the axis of symmetry. We treat this collective rotation in the adiabatic limit (for practical reasons), i.e. we assume that the effective potential energy for a cold nucleus without pairing can be written as the sum of intrinsic and rotational energies:

$$E(def, I) = E_{int}(def) + \frac{\hbar^2 I(I+1)}{2\Theta_{\perp}^{CM}(def)} \quad . \qquad (1)$$

As the superscript indicates, we employ the adiabatic cranking model (CM) expression $\theta_\perp^{CM}$ for the moment of inertia. The adiabaticity assumption also implies that the intrinsic energy E_{int} is only a function of deformation, but not of the angular momentum $I\hbar$. This approximation becomes less important the more the nucleus is excited, because the maximum I it can tolerate decreases with increasing excitation.

When BCS pairing is included, E_{int} and $\theta_\perp^{CM}$ depend also on the gap parameters Δ_n and Δ_p for neutrons and protons. Due to the assumption of adiabaticity, the CAP effect is not directly accessible in our approach, but we approximate it by a prescription discussed in Appendix A1. For the case of a finite intrinsic angular momentum component M along the symmetry axis, the CAP effect has been studied by Moretto[5] .

2.3 EXCITATION

Since we want to describe the excitation of a compound system we assume its intrinsic degrees of freedom to be in thermal equilibrium characterized by a temperature T. This holds if the intrinsic relaxation time is smaller than the fission lifetime. Support for intrinsic equilibration is provided by studies of strongly damped collisions[13] which dominate the reaction cross section for very heavy ions and seem to proceed on a shorter time scale than fusion-fission. Recent measurements of the energy spectra of neutrons evaporated from the reaction partners[13a] show that both fragments have the same temperature. Also, in a number of promising theoretical models[14] for such damped collisions, the intrinsic states have been treated statistically; sometimes the existence of a temperature is assumed.

Hence it seems justified to assume that true compound fission of a superheavy nucleus proceeds in thermal equilibrium.

With the assumptions made above, we can generalize eq. (1) and write the effective potential of a rotating heated nucleus in the macro-microscopic approach as

$$E(def, I, T) = E^{LDM}(def, T) + \delta E(def, T) + \frac{\hbar^2 I(I+1)}{2\,\Theta_{\perp}^{CM}(def, T)} \quad . \tag{2}$$

The first term is the energy of a heated liquid drop as discussed in sect. 5. Strutinsky's shell correction including a temperature-dependent pairing gap $\Delta(T)$ is the second term. In the rotational energy (last term), the moment of inertia also includes temperature and pairing effects. Explicit expressions will be given in the two subsequent sections. The quantitites δE and $\Theta_{\perp}^{CM}$ are evaluated separately for neutrons and protons and are then added.

2.4 ISOTHERMAL VERSUS ISENTROPIC PROCESSES

In thermodynamics, the pressure p of a system having volume V is given by the well-known relations

$$p = -\frac{\partial E(V,S)}{\partial V} = -\frac{\partial F(V,T)}{\partial V} \quad . \tag{3}$$

here, $F = E - TS$ is the free energy and S denotes the entropy. The first relation defines p, while the second is the equation of state (when F is known explicitly). Similarly, in a rotating heated nucleus the force in deformation space can be expressed by

$$\underset{\sim}{f} = -\underset{\sim}{\nabla}_{def} E(def, I, S) = -\underset{\sim}{\nabla}_{def} F(def, I, T). \qquad (4)$$

To make use of these relations, one has to specify a thermodynamic process for the deforming nucleus en route to fission with $I = const$. Physically, the appropriate function is not known and we must therefore resort to assumptions.

The isothermal process $T = const$ has usually been assumed in previous studies, because it is computationally the easiest to handle. In view of eq. (4), we stress that in this case the free energy

$$F(def, I, T) = E(def, I, T) - TS(def, T) \qquad (5)$$

is the associated effective potential rather than $E(def, I, T)$, which has often been used in the literature. Since usually only the deformation-dependent parts of the potentials are of interest, we infer from the last equation that F and E are equivalent in this respect only if S does not depend on deformation. In general, this condition is not fulfilled.

To keep T constant, heat energy must be delivered to or by the intrinsic system while the nucleus deforms. This can occur, for instance, when part of the collective kinetic energy is dissipated during rapid motion. In the adiabatic limit, however, $T = const$ implies the assumption of a (non-existent) thermal reservoir. Hence we conclude that the isentropic

process $S = const$ is the more realistic assumption in the adiabatic limit. In this case, we see from eq. (4) that $E(def, I, S)$ is the associated effective potential. To illustrate the differences between isothermal and isentropic processes, numerical comparisons will be given in sect. 7.

In order to calculate $F(def, I, T)$ and $E(def, I, S)$, the entropy $S(def, T)$ must be known. We use a macro-microscopic expression analogous to E, namely

$$S(def, T) = S^{LDM}(def, T) + \delta S(def, T) , \tag{6}$$

the constituents of which will be derived further below. As a consequence of the adiabaticity assumption, S does not depend on I, provided the entropy created by rotation can be neglected. Inserting eqs. (2,6) into eq. (5), we arrive at the effective potential for the isothermal process:

$$F(def, I, T) = F^{LDM}(def, T) + \delta F(def, T) + \frac{\hbar^2 I(I+1)}{2\Theta_\perp^{CM}(def, T)} , \tag{7}$$

where $F^{LDM} = E^{LDM} - TS^{LDM}$ and $F = E - TS$.

To describe the isentropic process, eq. (6) must be solved (numerically) for $T(def, S)$. Inserting this into eq. (2), we get the isentropic effective potential $E(def, I, S) \equiv E(def, I, T(def, S))$ or explicitly

$$E(def,I,S) = E^{LDM}(def,S) + \delta E(def,S) + \frac{\hbar^2 I(I+1)}{2\,\Theta_I^{cm}(def,S)} \quad . \tag{8}$$

An example for the determination of the temperature in an isentropic process is provided by Fig. 1. The entropy increases almost linearly with temperature for constant deformation. It can be seen that the difference between the isentropic and isothermal processes is most pronounced for moderate temperatures about 0.5...1 MeV. At higher excitations, the entropy changes little with deformation but the isentropic temperature is systematically higher than the spherical one.

3. Temperature-dependent BCS model

3.1. INTRINSIC STATISTICAL QUANTITIES

In the following we give explicit expressions for various quantities entering the shell corrections. We start from the well-known BCS Hamiltonian with constant pairing strength G, written in second quantization form:

$$H^{BCS} = \sum_k \varepsilon_k a_k^\dagger a_k - G \sum_{k,k'>0} a_{-k}^\dagger a_k^\dagger a_{k'} a_{-k'} \quad . \tag{9}$$

Here, $k = \pm 1, \pm 2, \ldots$ labels the quantum numbers of the single-particle states $|k\rangle$ with energy $\varepsilon_k = \varepsilon_{-k}$, the state $|-k\rangle$ being the time reverse of $|k\rangle$. For the s.p. Hamiltonian to be specified in sect. 6, the states depend on deformation and $|k\rangle$, $|-k\rangle$ have opposite projections of the s.p. angular momentum along the symmetry axis. Though not explicitly indicated, the pairing

force is allowed to act only in an energy interval around the Fermi level; otherwise $G=const$ would be a meaningless approximation.

To introduce thermal excitation, we employ the grand canonical formalism, following refs.[4,5]. In principle, the s.p. states $|k\rangle$ depend on temperature, but this effect can safely be neglected[15]. With some approximations, the grand potential Ω for one type of nucleons (neutrons or protons) resulting from H^{BCS} can be expressed as

$$\Omega = -T \ln \mathcal{Z}$$

$$= \sum_{k>0} (\varepsilon_k - \lambda - e_k) - 2T \sum_{k>0} \ln \left[1+\exp\left(-\frac{e_k}{T}\right)\right] + \frac{\Delta^2}{G} \,. \tag{10}$$

Here, $\mathcal{Z}$ is the grand partition function and the temperature T is measured in energy units. Quasi-particle energies are denoted by $e_k = [(\varepsilon_k-\lambda)^2 + \Delta^2]^{1/2}$. The gap parameter $\Delta(T)$ and the chemical potential $\lambda(T)$ are determined by the coupled gap and particle number conservation equations

$$\mathcal{N} = N \text{ or } Z$$

$$\frac{2}{G} = \sum_{k>0} \frac{1}{e_k} \tanh \frac{e_k}{2T} \,. \tag{11}$$

In the grand ensemble, the following general expressions hold for the average particle number, energy, entropy and free energy:

$$N = -\frac{\partial \Omega}{\partial \lambda}$$

$$E = \frac{\partial (\Omega/T)}{\partial (1/T)} + \lambda N$$

$$S = -\frac{\partial \Omega}{\partial T} = \frac{-\Omega + E - \lambda N}{T}$$

$$F = E - TS. \qquad (12)$$

Inserting Ω from eq. (10) we obtain the explicit forms

$$N^{BCS}(def,T) = \sum_{k>0} \left[1 - \frac{\varepsilon_k - \lambda}{e_k} \tanh \frac{e_k}{2T}\right] ,$$

$$E^{BCS}(def,T) = \sum_{k>0} \varepsilon_k \left[1 - \frac{\varepsilon_k - \lambda}{e_k} \tanh \frac{e_k}{2T}\right] - \frac{\Delta^2}{G} ,$$

$$S^{BCS}(def,T) = 2 \sum_{k>0} \left[\ln\left(1+\exp\left(-\frac{e_k}{T}\right)\right) + \frac{e_k/T}{1+\exp(e_k/T)}\right] ,$$

$$F^{BCS}(def,T) = E^{BCS}(def,T) - TS^{BCS}(def,T).$$

(13)

Though not shown explicitly, all quantities on the right (except T) depend on deformation. In the limit $T=0$, $G_1=0$, the energy becomes the sum of the ε_k over occupied states, while $S=\Delta=0$ and $F=E$. When G_1 is finite and T is increased, $\Delta(T)$ decreases monotonically until the pairing correlation vanishes at a critical temperature $T_{crit} \approx (0.5 \ldots 1)\,MeV$, see e.g. ref.[5]) for further details. An example of this phase transition is given in Fig. 2.

3.2 CRANKING-MODEL MOMENT OF INERTIA

When a Hartree-Fock Hamiltonian is cranked adiabatically about the i-th body-fixed axis of the nucleus with angular velocity ω_i, one defines the moment of inertia as

$$\Theta_i^{CM} = \frac{\hbar}{\omega_i} \mathrm{Tr}\; J_i\, h^{(1)}. \tag{14}$$

Here J_i is the i-th component of the total angular momentum operator and $h^{(1)}$ is the difference of the s.p. density operators for $\omega_i \neq 0$ and $\omega_i = 0$. The resulting well-known Inglis expression can be generalized to include temperature-dependent pairing. In good approximation, the moment of inertia can be written as [3,16)]

$$\Theta_i^{CM}(def,T) = \frac{\hbar^2}{2} \sum_{k,k'} |\langle k|\hat{j}_i|k'\rangle|^2 \cdot \left[\frac{(u_k v_{k'} - v_k u_{k'})^2}{e_k + e_{k'}} \left(\tanh\frac{e_k}{2T} + \tanh\frac{e_{k'}}{2T} \right) + \frac{(u_k u_{k'} + v_k v_{k'})^2}{e_k - e_{k'}} \left(\tanh\frac{e_k}{2T} - \tanh\frac{e_{k'}}{2T} \right) \right]. \tag{15}$$

Here u_k and v_k are the usual BCS amplitudes and $\hat{j}_i$ is the i-th component of the s.p. angular momentum operator. We repeated the explicit expression (15) here because it was misprinted in both references quoted above.

4. Strutinsky renormalization

4.1. SHELL CORRECTIONS TO INTRINSIC QUANTITIES

Following ref.[4] we define the shell-plus-pairing correction to the intrinsic energy for $T \geq 0$ and for one type of nucleons as

$$\delta E(def,T) = E^{BCS}(def,T) - \tilde{E}^{BCS}(def,T) . \tag{16}$$

The second term is the smooth energy

$$\tilde{E}^{BCS}(def,T) = \int_{-\infty}^{\infty} d\varepsilon \; g(\varepsilon)\varepsilon \left[1 - \frac{\varepsilon-\tilde{\lambda}}{\tilde{e}(\varepsilon)} \tanh \frac{\tilde{e}(\varepsilon)}{2T} \right] - \frac{\tilde{\Delta}^2}{G} , \tag{17}$$

obtained from eq. (11) by averaging over an energy interval $\tilde{\gamma}$ (of the order of a major shell spacing) with the smoothed level density

$$g(\varepsilon) = \frac{1}{\sqrt{\pi}\,\tilde{\gamma}} \sum_{k>0} \exp\left[-\left(\frac{\varepsilon-\varepsilon_k}{\tilde{\gamma}} \right)^2 \right] F_6\left(\frac{\varepsilon-\varepsilon_k}{\tilde{\gamma}} \right) . \tag{18}$$

The curvature correction function F_6 in this expression is given explicitly in Appendix A2. The smooth quasi-particle energy in eq. (17) is defined as $\tilde{e}(\varepsilon) = \left[(\varepsilon-\tilde{\lambda})^2 + \tilde{\Delta}^2 \right]^{1/2}$. Further, the

chemical potential $\tilde{\lambda}(T)$ and the gap $\tilde{\Delta}(T)$ are determined by the smoothed versions of eqs. (11). Since the numerical solution of these coupled integral equations for each deformation is rather time consuming, we use instead of eq. (16) the approximation

$$\delta E(def,T) \approx E^{BCS}(def,T,\Delta) - \tilde{E}^{BCS}(def,T,\Delta=0) . \tag{19}$$

We have numerically estimated that the resulting error should be negligible, aside from a constant shift, which is independent of deformation and therefore irrelevant because we are only interested in the deformation energy. Thus we have to solve only eqs. (11) for $\lambda(T)$, $\Delta(T)$ and the smoothed particle number equation yielding $\tilde{\lambda}(T)$ with $\Delta=0$ fixed.

We further define the shell correction to the entropy

$$\delta S(def,T) = S^{BCS}(def,T) - \tilde{S}^{BCS}(def,T) , \tag{20}$$

and to the free energy

$$\delta F(def,T) = \delta E(def,T) - T\,\delta S(def,T) . \tag{21}$$

Here, $\tilde{S}$ is the smooth entropy defined analogously to $\tilde{E}$. Some details as to the numerical calculation of the shell corrections using a Sommerfeld expansion are given in Appendix A.2.

4.2 SHOULD ONE RENORMALIZE THE MOMENT OF INERTIA?

In the spirit of the macro-microscopic approach it would seem natural to define a smooth moment of inertia $\tilde{\Theta}$ and a shell correction $\delta\Theta$ [cf. ref.[17]]. The problem, however, is that no classical expression for $\tilde{\Theta}$ is known which would reproduce on the average the experimental values found in low-energy spectroscopy. As is well known[18], the rigid-body moment $\Theta^{RB} \approx 2\Theta^{exp}$, while the irrotational flow value Θ^{IF} underestimates Θ^{exp} by about a factor of 5. Whereas irrotational flow is obviously an unrealistic assumption, the failure Θ^{RB} is due to the pairing interaction, because Θ^{RB} seems to be a good approximation when pairing has vanished at large excitation and/or angular momentum.

On the other hand, the cranking value Θ^{CM} with pairing included underestimates Θ^{exp} only by about 10-20%, see e.g. ref.[18]. Further, the necessity to renormalize Θ^{CM} is less obvious than in the case of the deformation energy obtained by summation of the $\varepsilon_k(def)$, for the following reason. The well-known deficiencies of the latter method arise because the usual prescription (namely, keeping the volume of the equipotential surfaces of the s.p. potential constant under deformation) simulates only inadequately the constancy of the density volume. In contrast, Θ^{CM} depends essentially on differences of the ε_k. This is easily seen in the limit $T=\Delta=0$ of eq. (15) which is the Inglis formula. Therefore Θ^{CM} is much less sensitive to any unrealistic behaviour of $\varepsilon_k(def)$ than the sum of the ε_k and we use Θ^{CM} as given by eq. (15).

A second problem concerning θ^{CM} arises when the s.p. Hamiltonian contains momentum-dependent terms such as the $\underset{\sim}{\ell}\cdot\underset{\sim}{s}$-potential or the ℓ^2-correction term in Nilsson type Hamiltonians. In this case, θ^{CM} exceeds θ^{RB} for sufficiently large temperatures (i.e. $\Delta=0$) by about 40%, see Fig. 3. This undesirable effect has also been observed earlier[19] and is mostly due to the ℓ^2-term, which is also present in our Hamiltonian. The effect of spin-orbit and ℓ^2-terms on the perpendicular moment of inertia can be seen in Table 1. A corresponding renormalization has been proposed in ref [8], but we think that one should rather modify the ℓ^2-term. Since the momentum effects alter the critical angular momenta only by about 20% for the nuclei considered here, we have made no attempt to renormalize θ^{CM} in this respect, either.

5. Liquid drop model with finite temperature

A consistent generalization of the macro-microscopic method to include excitation requires a liquid drop model (LDM) describing a heated nucleus. This is because the volume and surface area increase with the temperature of the drop, while the density $n(T)$ and the surface tension $\sigma(T)$ decrease. These effects are not accounted for in the shell correction derived in the last section. We employ the T-dependent LDM of ref.[20], which is based on a Thomas-Fermi description[21] of the excited nucleus. Essentially the same results have been obtained with a Hartree-Fock treatment in ref.[22]. For the temperature range $0\leq T\leq 2\,MeV$ considered here, the following approximate expressions were given in ref.[20]

$$n(T) = n(0)\left(1-\alpha T^2\right), \qquad \alpha = 0.0032\ MeV^{-2}$$

$$\sigma(T) = \sigma(0)\left(1-\beta T^2\right), \qquad \beta = 0.0114\ MeV^{-2}$$

$$x(T) = x(0)\,\frac{\sigma(0)\,n(T)}{\sigma(T)\,n(0)} \approx x(0)\left(1+(\beta-\alpha)T^2\right). \tag{22}$$

Here $x(0)$ is the usual fissility parameter which becomes a function $x(T)$ for a heated drop.

We start by decomposing the free energy F into its volume, surface, and Coulomb parts, respectively:

$$F^{LDM}(def,T) = F_{vol}^{LDM}(T) + F_{surf}^{LDM}(def,T) + F_{Coul}^{LDM}(def,T). \tag{23}$$

For a spherical drop, this equation can also be written as

$$F^{LDM}(sph,T) = F_{vol}^{LDM}(T) + F_{surf}^{LDM}(sph,T)\left[1+2x(T)\right], \tag{24}$$

which shows the meaning of the T-dependent fissility. For the remainder of this section, we drop the superscript LDM for brevity, as all quantities refer to the liquid drop. Once $F(def,T)$ is known explicitly, all other quantities of interest follow immediately (see below).

The volume part of F can be derived from Stocker's model[23] of heated nuclear matter. In good approximation it is given by

$$F_{vol}(T) = E_{vol}(0)\,\frac{n(0)}{n(T)} \approx E_{vol}(0)\left(1+\alpha T^2\right), \tag{25}$$

where $E_{vol}(0) = -(16\,MeV)\,A$ denotes the usual LDM volume energy. Note that both F_{vol} and E_{vol} do not depend on deformation. Next we recall[20] that the surface tension σ is the free energy of the surface layer per unit area. Thus we can express the surface part of F as

$$F_{surf}(def,T) = E_{surf}(def,0)\;\frac{\sigma(T)}{\sigma(0)}\left(\frac{n(0)}{n(T)}\right)^{2/3}$$

$$\approx E_{surf}(def,0)\left(1-(\beta-2\alpha/3)T^2\right). \tag{26}$$

The first factor is the usual LDM surface energy proportional to the surface area. Further, the Coulomb part of F is taken as

$$F_{Coul}(def,T) = E_{Coul}(def,0)\left(\frac{n(T)}{n(0)}\right)^{1/3}$$

$$\approx E_{Coul}(def,0)\left(1-\tfrac{1}{3}\alpha T^2\right), \tag{27}$$

where $E_{Coul}(def,0)$ is the usual LDM Coulomb energy.

Having specified F explicitly, we arrive at the free deformation energy for the isothermal process, normalized to zero for the spherical shape:

$$F^{def}(def,T) = F(def,T) - F(sph,T)$$

$$= E_{surf}^{def}(def,0)\left(1-(\beta-2\alpha/3)T^2\right) + E_{Coul}^{def}(def,0)\left(1-\tfrac{1}{3}\alpha T^2\right), \qquad (28)$$

where the surface and Coulomb energies have been normalized analogously. Since $\beta>\alpha$, the isothermal LDM barrier F^{def} is lowered when the temperature rises.

The entropy S is obtained from the thermodynamical relation $S(def,T) = -\partial F(def,T)/\partial T$ as the sum

$$S(def,T) = 2T\left(-\alpha E_{vol}(0) + (\beta-2\alpha/3)E_{surf}(def,0) + \tfrac{1}{3}\alpha E_{Coul}(def,0)\right) \qquad (29)$$

over volume, surface and Coulomb contributions, respectively. Finally, the internal energy is determined by $E(def,T) = F(def,T) + TS(def,T)$. Only for the isothermal process, its deformation-dependent part is given by

$$E^{def}(def,T) = E_{surf}^{def}(def,0)\left(1+(\beta-2\alpha/3)T^2\right) + E_{Coul}^{def}(def,0)\left(1+\tfrac{1}{3}\alpha T^2\right). \qquad (30)$$

As expected, the deformation energy increases with temperature.

For the isentropic process $S=const$ within the pure LDM picture, the energy as function of deformation and S is also

needed, see sect. 2.4. This is obtained easily observing that eq. (29) can be solved analytically for $T(def, S)$. For constant S, the temperature in the fissioning drop decreases because the dominant deformation dependence in eq. (29) comes from the increasing surface term. When both the isothermal and the isentropic process are started in the spherical state with the same excitation characterized by T_{sph} this cooling effect causes the isentropic barrier to rise less rapidly than the energy in eq. (30). Further, it will be shown that the isentropic barrier for finite T_{sph} is always higher than the isothermal one.

Lastly we note that the rigid-body moment of inertia of the drop is but a very weak function of T. From the above model, we find

$$\Theta^{RB}(def,T) \simeq \Theta^{RB}(def,0)\left(1+\tfrac{2}{3}\alpha T^2\right). \qquad (31)$$

In the temperature range $0 \le T \le 2\,MeV$ under consideration, Θ^{RB} increases by about 1%. A similar observation[8] has been made for Θ^{CM} obtained from cranking without pairing.

6. Shape parameterization and single-particle Hamiltonian

We employ the Lawrence[24] family of symmetric fission shapes which has been used extensively in liquid drop fission calculations[25] and in connection with a s.p. potential of finite depth, including the mass asymmetry degree of freedom[3]. A two-center shell model Hamiltonian corresponding to these shapes has been constructed by Albrecht[24], who also proposed a convenient parameterization of Lawrence's family. Both have

been applied in the present calculations. Only the major properties will be recalled here; full details can be found in ref.[26].

6.1 SHAPE PARAMETERIZATION

Figure 4 illustrates the family of shapes in terms of the separation (or elongation) parameter s and the constriction (or necking-in) parameter c. In cylindrical coordinates, the surface of the drop is given by

$$\rho^2(z;s,c) = \left[(R_0\lambda)^2 - \left(\frac{z}{s+1}\right)^2\right]\left[\left(\frac{c}{s+1}\right)^2\left(\frac{z}{R_0\lambda}\right)^2 + g_m(c)\right]$$

$$g_m(c) = \begin{cases} 1 & \text{for } c \le 1 \\ c(2-c) & \text{for } c \ge 1 \end{cases} . \qquad (32)$$

The factor $\lambda(s,c)$ takes care of volume conservation under deformation. For small values of s and c, Lawrence shapes are similar to Nilsson shapes with parameters ε and ε_4. In the pure LDM model, the main fission direction (LDM valley) is given by $s \approx c$. The corresponding liquid drop potential energy surface for a superheavy nucleus is shown in Fig. 5.

6.2 SINGLE-PARTICLE HAMILTONIAN

In cylindrical coordinates ρ, z, our single-particle potential is given by

$$V(\rho,z;s,c) = \frac{m}{2}\omega_0^2\left[\rho^2 + (1-\gamma)z^2 + \frac{\eta}{(\lambda R_0)^2}z^4\right] + V_0\left(1 - g_m(c)\right) . \qquad (33)$$

The deformation dependent auxiliary quantities $\omega_0(s,c)$, $\gamma(s,c)$, $\eta(s,c)$, $\lambda(s,c)$ and the constant V_0 are defined in ref.[26], where also illustrations of the potential may be found. For $c=0$, our V is a spherical Nilsson oscillator potential (ε-degree of freedom). Necking-in begins at $c=1$. For each deformation, all equipotential surfaces have Lawrence shapes.

The full s.p. Hamiltonian is

$$H^{sp} = \frac{\underset{\sim}{p}^2}{2m} + V - \hbar\omega_0 \varkappa \left(\underset{\sim}{\nabla} (V/\tfrac{1}{2}\hbar m\omega_0) \times \underset{\sim}{p} \right) \cdot \underset{\sim}{s}$$

$$- \hbar\omega_0 \varkappa \mu \left(\ell^2 - \tfrac{1}{2} N(N+3) \right) . \qquad (34)$$

It includes a Thomas-type spin-orbit term and an ℓ^2-correction term with strength coefficients $\varkappa(c)$ and $\mu(c)$.

All numerical parameters H^{sp} as well as the LDM constants and the strength and range of the pairing interaction are the same as in ref.[26]. We assume here that the pairing strength G_τ is proportional to the nuclear surface area. The fission barriers of superheavy elements which result from this choice, in the case $T=0$, $I=0$ are those of the more pessimistic estimate of Gustafsson[27].

7. Results and discussion

We have applied the model described above to the following superheavy systems

$$^{270}_{160}110 = {}^{84}_{48}Kr + {}^{186}_{112}W, \quad {}^{278}_{168}110 = {}^{40}_{22}Ar + {}^{238}_{146}U,$$

$$^{292}_{174}118 = {}^{84}_{48}Kr + {}^{208}_{126}Pb, \quad {}^{298}_{184}114, \quad {}^{322}_{194}128. \tag{35}$$

The first three systems were selected because the indicated heavy-ion reactions have been studied experimentally[28] at various bombarding energies E_{cm}. From the measured complete fusion cross sections $\sigma_{CF}(E_{cm})$, angular momenta $\ell_{CF}(E_{CM})$ were derived using the sharp cut-off model, where $\sigma_{CF} = \pi\lambda^2(\ell_{CF}+1)^2$. The experimental ℓ_{CF} depends on entrance channel effects[13] and includes particle evaporation and fission processes occurring where the projectile has transferred its full momentum. Since we do not know at present which fraction of σ_{CF} refers to true compound processes, it would be rather meaningless to compare these ℓ_{CF} values to our I_{cr} given below. It is not even clear whether $\ell_{CF}(E_{cm})$ should be larger than I_{cr} at the corresponding compound nucleus excitation energy E^*. This is because due to the reaction dynamics, the compound stage might not be reached, although it could be able to tolerate more angular momentum than offered by ℓ_{CF}. In the experiments quoted, the bombarding energies were about 50...200 MeV above the Coulomb barrier. From this one can estimate[29] that the maximum temperature varies between 1 and 2.5 MeV.

The system $^{298}114$ is considered here because it has been predicted by various authors[12] to be the superheavy nucleus most stable against fission. It is less neutron deficient than the other three systems and therefore it can probably not be reached directly in a fusion reaction. The dependence of its barrier on angular momentum has been studied before in refs.[6,8].

7.1. ENTROPY, SHELL CORRECTIONS, AND MOMENTS OF INERTIA

As already indicated in Fig. 1, the difference between isothermal and isentopic processes is most pronounced for moderate temperatures, $T \approx 0.5$ MeV. Since the liquid drop contribution to the entropy is a smooth function of deformation, this effect is caused by the shell correction to the entropy. From Fig. 6, it can be seen that for the system $^{292}118$ at this very temperature the correction is negative for small deformations ($\varepsilon \approx -0.2 \ldots +0.2$) and positive for large deformations ($\varepsilon \approx 0.8$). This comes from the fact that the magic nucleus $^{292}118$ at sphericity has a low-level density above the Fermi energy, whereas at large deformation deformed shells come into play and generate a large level-density about the Fermi energy. The shell correction to the entropy vanishes for the cold nucleus (entropy is zero) and also for higher temperatures ($T \approx 2$ MeV), as soon as the range of the temperature-smeared out Fermi-surface becomes comparable to the range of the Strutinsky averaging procedure.

The same effect of the level density is observed in the shell correction to the energy and to the free energy, Fig. 7, with the exception that these shell corrections need not vanish at $T=0$. There exists, however, a well-pronounced difference

between $\delta E(T)$ and $\delta F(T)$, namely that at small (large) deformation δF is increasing (decreasing) monotonically with temperature rather than having a minimum (maximum) as does δE. According to eq. (21) the extrema in δE here are cancelled by the term $-T\delta S$ to give a smooth dependence of δF on T. For nonmagic nuclei, again the level density above the Fermi-surface determines the behaviour of the shell corrections with respect to temperature and deformation.

The shell effects of the entropy create local temperature extrema for the isentropically deforming nuclear system. At deformations which correspond to potential minima (maxima) the temperature exhibits maxima (minima), cf. Fig. 8. In addition, the increase of surface energy during deformation causes a slight cooling of the isentropic liquid drop, cf. eq. (29). As will be shown below, this cooling is of the order of 15% at the second barrier and enhances the isentropic barrier heights.

The drastic dependence of the moment of inertia on deformation and temperature can be seen in the contour plot of Fig. 9. Here it is interesting to note for which kind of shapes the moment of inertia becomes maximal. For the hot nucleus where shell effects are already washed out, these are long ellipsoidal shapes just as for the classical drop. In the cold nucleus the shell effects give rise to large moments of inertia corresponding to compact cylindrical shapes. This gives rise to a shift of the position of the fission barrier and, consequently, to a different fission path for the rotating nucleus as compared to the former case.

7.2. EXCITED, NONROTATING SYSTEMS

The influence of temperature on the potential energy surface for isothermal and isentropic processes can be seen in the contour plots, Figs. 10, 11. Three features can be observed. First, for increasing temperatures, the isothermal and isentropic barriers move towards more compact shapes. This results mostly from the behaviour of the moments of inertia as discussed above. Secondly, the isothermal barriers are in general lower than the isentropic ones because the contribution of the entropy to the energy partly cancels the shell effects and, also, because the corresponding LDM energies are lower. As a consequence, the isentropic barriers do not necessarily decrease monotonically with temperature as the isothermal ones do. This trend can be seen for $^{270}110$ in the lower part of Fig. 12, where the deformation energy along the fission path is shown, and for $^{270}110$ and $^{278}110$ in Table 2.

The resulting barrier heights and depths of the second minima are listed in Table 2. In order to compare our results with those of other groups, we also include in this table barrier heights obtained if pairing is omitted (lower lines). Generally, barriers are lower when pairing is included because it acts like a temperature in smearing out the occupation numbers about the Fermi level and thus attenuates the shell correction. Our result for the barrier height of $^{298}114$ omitting pairing, for instance, is somewhat lower than the value 12.1 MeV of Andersson et al.[8] who used a Nilsson model, and with pairing included it is much lower than the value 8.5 MeV of Mustafa and Kumar[6].

The table gives only barrier heights for temperatures up to 1.5 MeV. Apart from the system $^{298}114$ which still has a small barrier at $T=2\,MeV$, no barriers were found in the other systems under consideration for such high temperatures.

7.3. ROTATING, COLD SYSTEMS

A temperature of about 0.6 MeV causes pairing to break down, cf. Fig. 2. Hence, in discussing the behaviour of rotating but cold nuclear systems, pairing plays an essential role. In particular, the Coriolis antipairing effect is most pronounced in cold nuclei, and barrier heights depend strongly on the degree of pairing. This is illustrated in Fig. 13, where the barrier heights of $^{270}110$ are plotted if pairing is not admitted and if CAP effects are taken into account as described in Appendix A.1. It can be seen that the CAP effect essentially lowers the barriers compared to the case $\Delta=0$. Both curves coincide from $I=60\hbar$ on, which means that all pairs are broken at all deformations. For higher angular momenta, the barrier height is decreasing monotonically until the critical angular momentum is reached. The latter is defined as the value of I where the barrier height is approximately 0.2 MeV.

The resulting large critical angular momenta for the cold systems listed in the first column of Table 3 are unrealistic because such compound nuclei without excitation energy cannot be produced in a heavy-ion reaction. The system $^{298}114$, for instance, can carry an angular momentum of $184\hbar$. This is of the same order as the result of the calculations of Andersson et al.[8] for the same system but with inclusion of triaxial

shapes. They obtained a barrier height of 1 MeV for $I=100$, thus $I_{cr}>100$. The value $I_{cr}=32$ of Mustafa and Kumar[6], on the other hand, is not compatible with either calculation.

7.4. EXCITED, ROTATING SYSTEMS

The interesting temperature range in heavy-ion collisions well above the Coulomb barrier is $1\,MeV \lesssim T \lesssim 2.5\,MeV$. For these temperatures (or T_{sp} in the isentropic case), the pairing force and, hence, also the CAP effect is ineffective. At $T \gtrsim 1.5\,MeV$ the critical angular momenta are substantially lower than the respective values for the cold nuclei. They are comparable to the results obtained with the pure rotating liquid drop model at $T=0$; cf. the entries in the last column of Table 3. Furthermore, since isentropic barriers are higher than isothermal ones, also isentropic I_{cr}-values are larger than isothermal ones.

A direct comparison of our static critical angular momenta with the experiment is not possible because fusion cross sections and, hence, experimental critical angular momenta depend on the dynamics of the entrance channel; for reviews on this subject cf. refs.[28,30,31] Present analyses[28] with great success make use of rotating liquid drop model fission barriers. Although for the excitation energies under consideration shell effects are diminished considerably by excitation and rotation, however, there remain corrections to the rotating liquid drop model from moments of inertia, temperature and entropy.

7.5. SUMMARY OF RESULTS

By use of a single-particle model with excitation and Strutinsky's renormalization procedure to the liquid drop model, we calculated shell corrections and cranking model moments of inertia. With help of these, the potential energy surfaces for the isentropic process and the free energy surfaces for the isothermal process have been studied in dependence on excitation (temperature) and rotation (angular momentum).

As results we first note that the physically more appropriate isentropic process, where no heat energy can be delivered to nor extracted from the system, always gives larger fission barriers because the energy shell correction is larger than the free energy shell correction and also because the associated LDM energy is higher for this process. Secondly, pairing is only important for temperatures below about 0.6 MeV if there is no rotation, or for angular momenta smaller than $60\hbar$, if there is no excitation. Already moderate excitation and rotation together cause the breakdown of pairing and of the Coriolis antipairing effect.

Further, the heavy systems of masses $270 \leq A \leq 322$ under consideration can tolerate surprisingly large angular momenta of the order of $I_{cr} \approx 140 \ldots 220$ when they are cold because then the shell effects are large. Unfortunately, this low-excitation regime is unaccessible for the production of superheavy nuclei. On the other hand, for temperatures typical of heavy-ion reactions well above the Coulomnb barrier, shell effects are greatly reduced, resulting in critical angular momenta of the order of the rotating liquid drop model results.

Appendices

A.1. THE CORIOLIS ANTIPAIRING EFFECT

At higher angular momenta the Coriolis force tends to break Cooper pairs, which results in a strong dependence of the moment of inertia $\Theta_{\perp}^{CM}(\Delta(I))$ on I via $\Delta(I)$. Krumlinde[32] suggested to treat this Coriolis antipairing effect by minimizing the effective potential energy, eq. (2), for each deformation with respect to the pairing gaps Δ_n, Δ_p. Since this can only be achieved at the expense of immense computer time, we approximated eq. (1) using two interpolation parameters δ_n (for neutrons) and δ_p (for protons). For each kind of nucleons, δ interpolates linearly between the cases $\Delta=0$ (no pairing) and the Δ corresponding to $I=0$ (maximum pairing). This interpolation is carried out for each deformation, temperature and angular momentum separately. Thus we have

$$0 \leq \delta_n(def, T, I),\ \delta_p(def, T, I) \leq 1. \qquad \text{(A1)}$$

We now suppress the arguments def, T for brevity but indicate the dependence on Δ explicitly. For the total energy in eq. (2), we then use the following interpolation formula:

$$E(I) = E^{n}_{int}(\Delta_n=0)(1-\delta_n) + E^{n}_{int}(\Delta_n(I=0))\,\delta_n$$

$$+ E^{p}_{int}(\Delta_p=0)(1-\delta_p) + E^{p}_{int}(\Delta_p(I=0))\,\delta_p$$

$$+ \tfrac{1}{2}\hbar^2 I(I+1)\left[\frac{1}{\Theta_n(\Delta_n=0)+\Theta_p(\Delta_p=0)}\left(1-\frac{\delta_n+\delta_p+|\delta_n-\delta_p|}{2}\right)\right.$$

$$+\frac{1}{\Theta_n(\Delta_n=0)+\Theta_p(\Delta_p(I))}\cdot\frac{\delta_p-\delta_n+|\delta_p-\delta_n|}{2}$$

$$+\frac{1}{\Theta_n(\Delta_n(I=0))+\Theta_p(\Delta_p=0)}\cdot\frac{\delta_n-\delta_p+|\delta_n-\delta_p|}{2}$$

$$\left.+\frac{1}{\Theta_n(\Delta_n(I))+\Theta_p(\Delta_p(I))}\cdot\frac{\delta_n+\delta_p-|\delta_n-\delta_p|}{2}\right]. \qquad \text{(A2)}$$

This expression is minimized with respect to δ_n, δ_p. The procedure for F is analogous.

A.2. SOMMERFELD EXPANSION

The expression for the particle number $\tilde{N}$ and the smoothed internal energy $\tilde{E}$ in the Strutinsky model at higher temperatures read [cf. eqs. (17,18)]

$$\tilde{N}^{BCS}(def,T,\Delta=0) = \frac{2}{\sqrt{\pi}\tilde{\gamma}}\sum_{k>0}\int_{-\infty}^{\infty} d\varepsilon\, e^{-u^2} F_6(u)\left(1+\exp\frac{\varepsilon-\tilde{\lambda}}{T}\right)^{-1} \qquad \text{(A3)}$$

$$\tilde{E}^{BCS}(def,T,\Delta=0)=\frac{2}{\sqrt{\pi}\tilde{\gamma}}\sum_{k>0}\int_{-\infty}^{\infty}d\varepsilon\,\varepsilon\,e^{-u^2}F_6(u)\left(1+\exp\frac{\varepsilon-\tilde{\lambda}}{T}\right)^{-1}, \tag{A4}$$

respectively, where $u=(\varepsilon-\varepsilon_k)/\tilde{\gamma}$ and

$$F_6(u)=\frac{35}{16}-\frac{35}{8}u^2+\frac{7}{4}u^4-\frac{1}{6}u^6 \tag{A5}$$

is the sixth order curvature correction.

As usual, $\tilde{\gamma}$, $\tilde{\lambda}$, T and ε_k denote the smearing width, smoothed Fermi energy, temperature, and single particle states, respectively. While these integrals can be solved in closed form for $T=0$, even a numerical computation for $T>0$ is tedious. This is because the implicit evaluation of $\tilde{\lambda}$ necessary for particle number conservation, $\tilde{N}=N$, requires a high accuracy in eqs. (A3,4) of about 10^{-5}. Therefore the Sommerfeld expansion[33]

$$\int_0^{\infty}dx\,\frac{d\varphi(x)}{dx}\left(1+e^{x-x_0}\right)^{-1}\approx\varphi(x_0)-\varphi(0)+\frac{\pi^2}{6}\left.\frac{d^2\varphi}{dx^2}\right|_{x=x_0} \tag{A6}$$

has been employed. If $x=\varepsilon/T$ and $x_0=\tilde{\lambda}/T$, this expansion holds for $T\ll\tilde{\lambda}$ in which case also the lower limit of the integral can be extended to $-\infty$. The final results are

$$\tilde{N}=\sum_{k>0}G_{76}(x), \tag{A7}$$

$$\tilde{E} = \sum_{k>0} \left(\varepsilon_k G_6(x) - \tilde{\gamma} G_8(x) \right) , \tag{A8}$$

where

$$G_{16}(x) = \frac{2}{\sqrt{\pi}} x e^{-x^2} \left[\frac{19}{16} - \frac{2}{3}x^2 + \frac{1}{12}x^4 - \frac{\pi^2 T^2}{6\tilde{\gamma}^2} \left(\frac{105}{8} - \frac{63}{4}x^2 + \frac{9}{2}x^4 - \frac{1}{3}x^6 \right) \right] + \operatorname{erfc}(-x) ,$$

$$G_{18}(x) = \frac{2}{\sqrt{\pi}} e^{-x^2} \left[\frac{5}{32} - \frac{15}{16}x^2 + \frac{5}{8}x^4 - \frac{1}{12}x^6 - \frac{\pi^2 T^2}{6\tilde{\gamma}^2} \left(\frac{35}{16} - \frac{35}{2}x^2 + \frac{35}{2}x^4 - \frac{14}{3}x^6 + \frac{1}{3}x^8 \right) \right] . \tag{A9}$$

Here $x = (\tilde{\chi} - \varepsilon_k)/\tilde{\gamma}$ and $\operatorname{erfc}(-x) = 1 + \operatorname{erf}(x)$ is the complementary error function with negative argument.

References

1. S. Cohen, F. Plasil and W.J. Swiatecki, Ann. Phys. (NY) 82 (1974) 557.
2. V.M. Strutinsky, Nucl. Phys. A95 (1967) 420.
3. H. Brack, J. Damgaard, A.S. Jensen, H.C. Pauli, V.M. Strutinski and C.Y. Wong, Rev. Mod. Phys. 44, (1972) 320.
4. A.S. Jensen and J. Damgaard, Nucl. Phys. A203 (1973) 578.
5. M. Sano and S. Yamasaki, Prog. Theor. Phys. 29 (1963) 397; L.G. Moretto, Nucl. Phys. A185 (1971) 145.
6. M.G. Mustafa and K. Kumar, Phys. Lett. 49B (1974) 405.
7. K. Neergård, V.V. Pashkevich and S. Frauendorf, Nucl. Phys. A262 (1976) 61.
8. G. Andersson, S.E. Larsson, G. Leander, P. Möller, S.G. Nilsson, J. Ragnarsson, S. Åberg, R. Bengtsson, J. Dudek, B. Nerlo-Pomorska, K. Pomorski and Z. Szymański, Nucl. Phys. A268 (1976) 205.
9. K. Neergård, H. Toki, M. Ploszajczak and A. Faessler, Nucl. Phys. A287 (1977) 48; M. Faber, M. Ploszajczak and A. Faessler, Nucl. Phys. A326 (1979) 129; R. Bengtsson, I. Hamamoto and R.H. Ibarra, Phys. Scripta 17 (1978) 583.
10. A.V. Ignatyuk, V.S. Stavinskii and Yu.N. Shubin, Yad. Fiz. 11 (1970) 1012; English transl. in Sov. J. Nucl. Phys. 11 (1970) 563.
11. S.E. Larsson, I. Ragnarsson and S.G. Nilsson, Phys. Lett. 38B (1972) 269.
12. T. Johansson, S.G. Nilsson and Z. Szymański, Ann. Phys. (Paris) 5 (1970) 377; P. Möller, Nucl. Phys. A192 (1972) 529; J.R. Nix, Ann. Rev. Nucl. Sc. 22 (1972) 65.

13. W.U. Schröder and J.R. Huizenga, Ann. Rev. Nucl. Sc. 27 (1977) 465; M. Lefort and Ch. Ngô, Ann. Phys. (Paris) 3 (1978) 5.

13a. D. Hilscher, J.R. Birkelund, A.D. Hoover, W.U. Schröder, W.W. Wilcke, J.R. Huizenga, A.C. Mignerey, K.L. Wolf, H.F. Breuer and V.E. Viola, Jr., Phys. Rev. C20 (1979) 576.

14. W. Nörenberg, Z. Physik A274 (1975) 241; D. Agassi, C.M. Ko and H.A. Weidenmüller, Ann. Phys. (NY) 107 (1977) 140; H. Hofmann and P. Siemens, Nucl. Phys. A257 (1976) 165; R.W. Hasse, Rep. Prog. Phys. 41 (1978) 1027.

15. M. Brack and Ph. Quentin, Phys. Scripta 10A (1974) 163.

16. J. Damgaard, H.C. Pauli, V.M. Strutinski, C.Y. Wong, M. Brack and A.S. Jensen, Proc. Second Int. Symp. on the Physics and Chemistry of Fission, Vienna 1969 (IAEA, Vienna 1969) p. 213.

17. V.V. Pashkevich and S. Frauendorf, Yad. Fiz. 20 (1974) 1122; English transl. in Sov. J. Nucl. Phys. 20 (1975) 588.

18. A. Bohr and B.R. Mottelson in "Nuclear Structure" (Benjamin, New York, 1975) vol. II, p. 74.

19. M. Brack and B.K. Jennings, Nucl. Phys. A258 (1976) 264.

20. R.W. Hasse and W. Stocker, Phys. Lett. 44B (1973) 26.

21. W. Stocker and J. Burzlaff, Nucl. Phys. A202 (1973) 265.

22. U. Mosel, P.-G. Zint and K.H. Passler, Nucl. Phys. A236 (1974) 252.

23. W. Stocker, Phys. Lett. 46B (1973) 59.

24. J.N.P. Lawrence, Phys. Rev. 139 (1965) B1227.

25. R.W. Hasse, Nucl. Phys. A128 (1969) 609.

26. K. Albrecht, Nucl. Phys. A207 (1973) 225.

27. C. Gustafsson, Proc. Int. Conf. on the Properties of Nuclei far from the Region of Beta-Stability, Leysin, 1970, ed. G. Rudstam (CERN-Report 70-30, Geneva, 1970) vol. 2, p. 654.

28. F. Plasil, Proc. Int. Conf. on Reactions between Complex Nuclei, Nashville 1974, ed. R.L. Robinson et al. (North-Holland, Amsterdam, 1974) vol. 2, p. 107.

29. J.M.B.Lang and K.J. LeCouteur, Proc. Phys. Soc. London A67 (1954) 586.

30. T.D. Thomas, Ann. Rev. Nucl. Sc. 18 (1968) 343.

31. A. Fleury and J.M. Alexander, Ann. Rev. Nucl. Sc. 24 (1974) 279.

32. J. Krumlinde, Nucl. Phys. A121 (1968) 306.

33. A. Sommerfeld, Z. Physik 47 (1928) 1.

Table 1

spin-orbit included		no	yes	yes
ℓ^2 included		no	no	yes
T in MeV	Δ	$\Theta_\perp^{CM}(T) / \Theta_\perp^{RB}(T)$		
0	>0	0.63	0.66	0.62
2	0	0.93	1.00	1.35

Effect of momentum-dependent terms in the single-particle Hamiltonian on the cranking moment of inertia. The example is $^{292}118$ with deformation $\delta=c=0.6$, which corresponds roughly to the second barrier. The entries give the cranking model perpendicular moments of inertia in units of the corresponding rigid body moment.

Table 2 Temperature dependence of barrier heights for I = 0.

System	T in MeV											
	0		0.5		1.0				1.5			
	I	II	I	II	I		II		I		II	
$^{270}_{110}$	3.7	0	2.3	0	3.7	1.7	0	0	0.9	0.2	0	0
	7.2	0.5	5.7	0								
$^{278}_{110}$	2.6	0.7	2.0	0	2.8	1.1	0	0	0.7	0	0	0
	6.4	0	4.7	0								
$^{298}_{114}$	5.6	1.8	4.0	0	2.6	1.3	1.3	0.3	1.0	0.4	0.2	0
	9.4	5.2	5.2	1.7								
$^{292}_{118}$	5.4	1.8	4.0	0	2.4	1.2	0.5	0	0.6	0.2	0	0
	8.6	3.5	5.2	1.7								
$^{322}_{128}$	8.0	0										
	13.8	0.3										

I: Height of maximum barrier in MeV with respect to the lowest minimum

II: Depth of the second minimum in MeV with respect to the lowest barrier

upper lines: Pairing included

lower lines: Pairing omitted

underlined values: Isentropic process

other values are for isothermal process or $T=0$.

Table 3 Critical angular momenta for various temperatures and for the rotating liquid drop.

System	T=0	1 MeV		1.5 MeV		2 MeV		RLDM
$^{270}_{110}$	140	70	56	45	0	0	0	32
$^{278}_{110}$	152	65	54	40	0	0	0	38
$^{298}_{114}$	184	60	50	35	16	15	0	20
$^{292}_{118}$	220	70	60	30	20	0	0	0
$^{322}_{128}$	200		50		30			0

The critical angular momenta are those values of I, where the barrier height is approximately 0.2 MeV. Values for isentropic processes are underlined, other entries refer to isothermal processes or $T=0$. The last column (RLDM) lists the critical angular momenta in the rotating liquid drop model[1] for $T=0$.

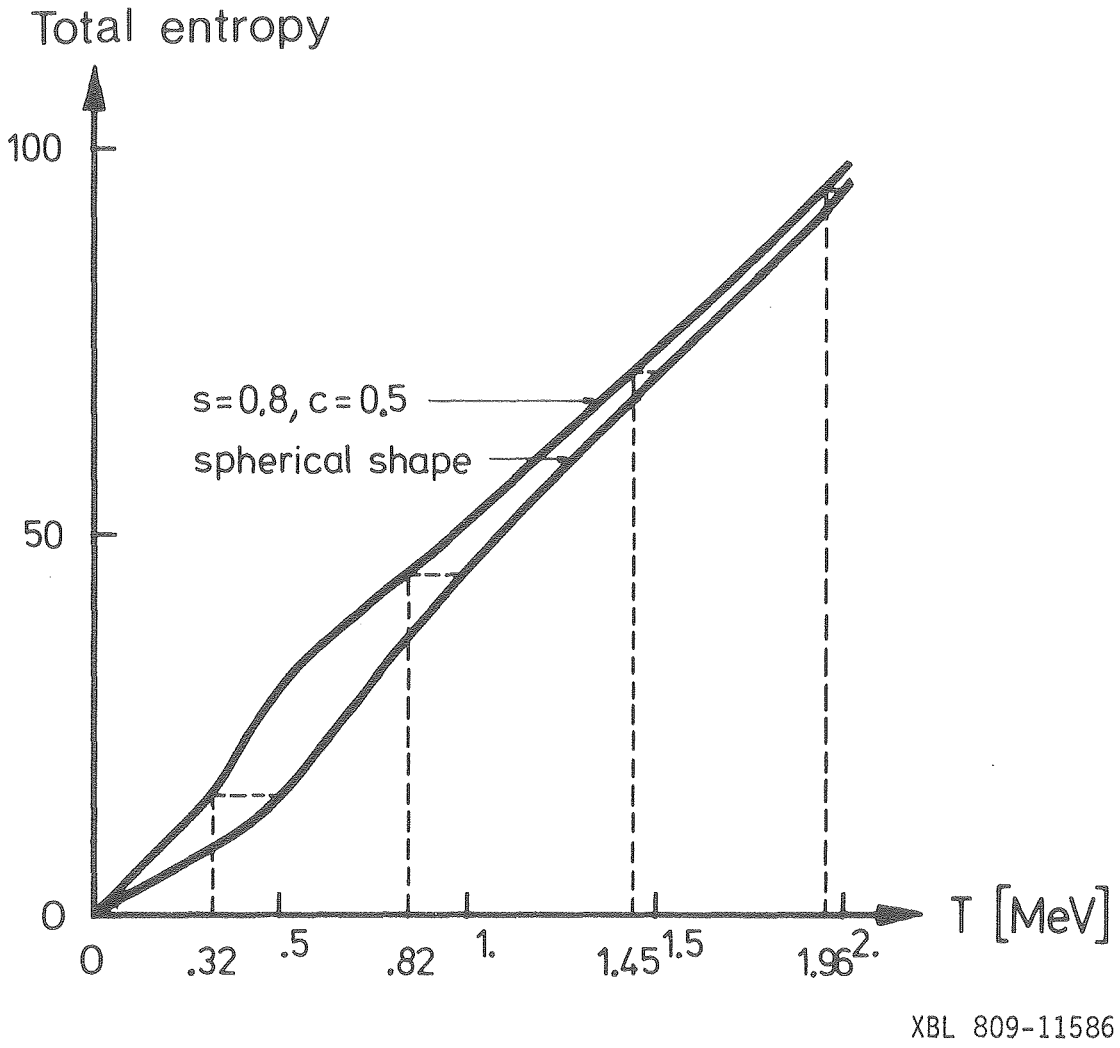

Fig. 1. Total (proton and neutron) entropies of spherical and deformed $^{292}118$ nuclei versus temperature. The parameters correspond to a deformation beyond the second barrier, cf. Fig. 4.

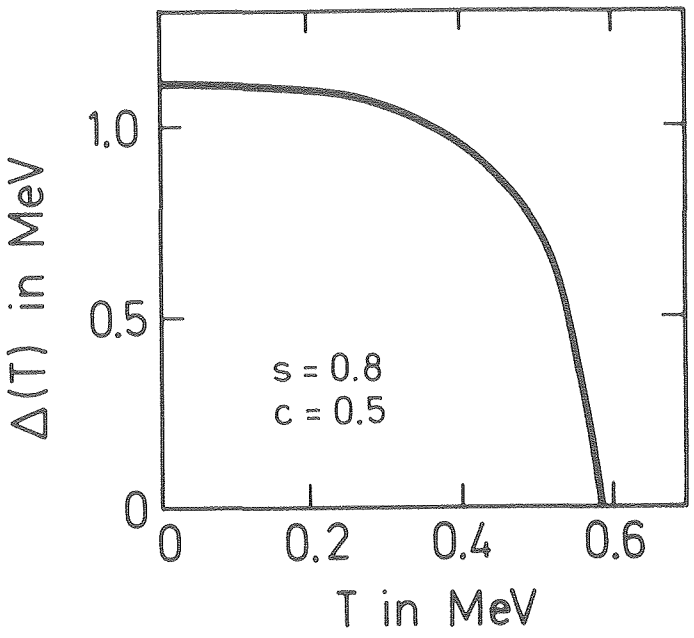

XBL 809-11587

Fig. 2. The neutron pairing gap of the compound nucleus $^{292}118$ versus temperature. The parameters indicated correspond to a deformation beyond the second barrier, cf. Fig. 4.

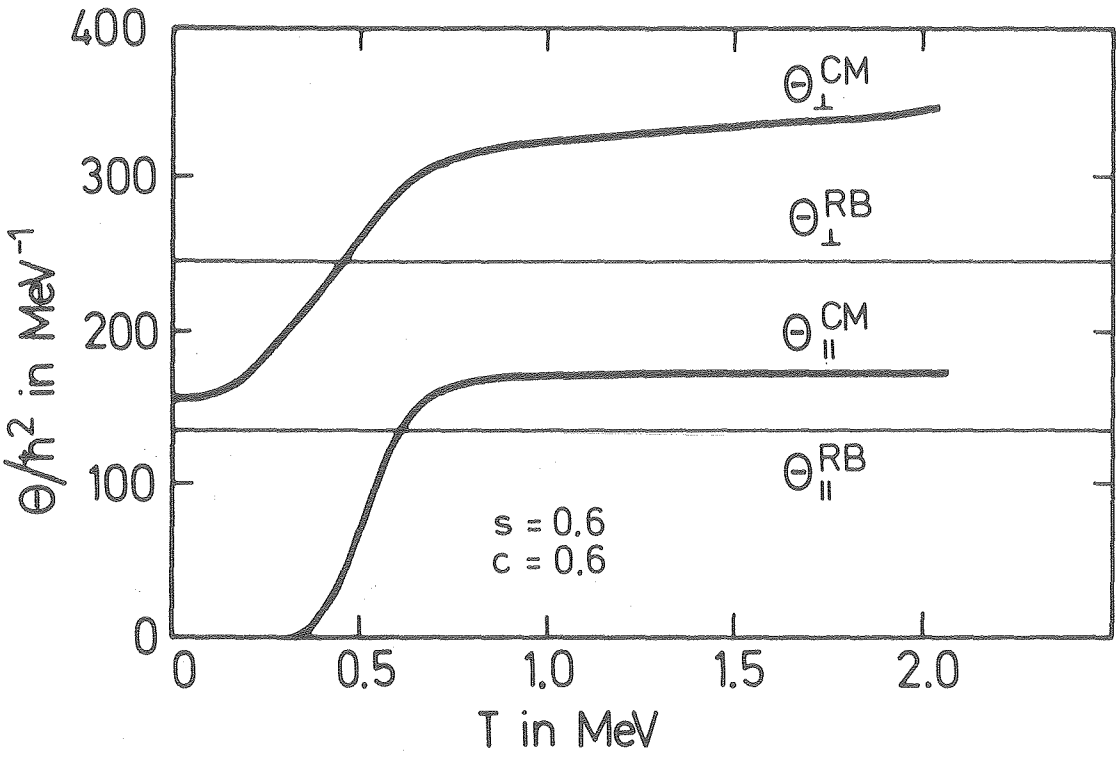

XBL 809-11588

Fig. 3. Cranking and rigid body total (protons and neutrons) moments of inertia perpendicular and parallel to the axis of symmetry for the compound nucleus $^{292}_{118}$ versus temperature. The parameters indicated correspond roughly to the deformation of the second barrier at a temperature of T = 1 MeV.

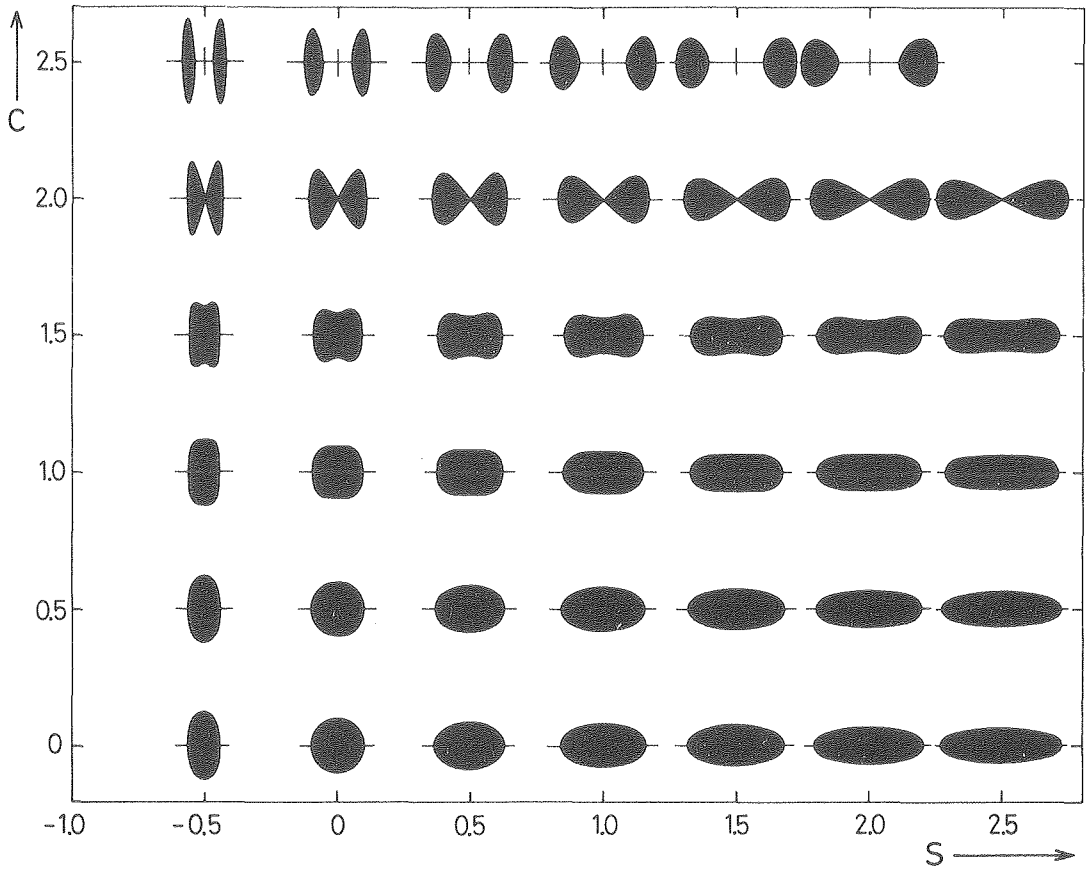

XBL 809-11589

Fig. 4. Examples of shapes contained in the parameterization, eq. (32).

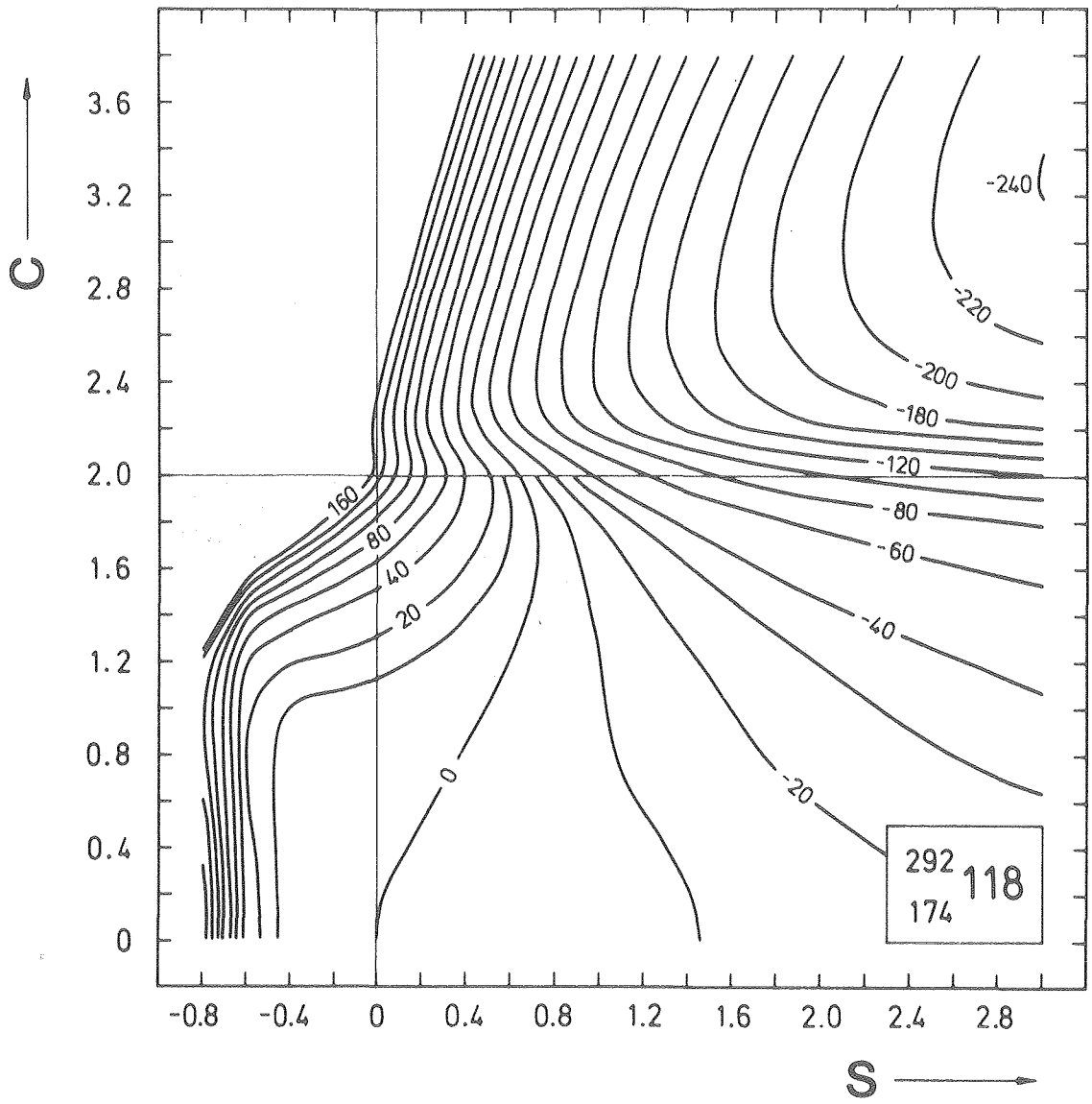

XBL 809-11590

Fig. 5. Liquid drop potential energy surface in the parameterization of eq. (32) for the cold ($T=0$) compound nucleus $^{292}118$. This heavy nucleus does not have a liquid drop minimum nor a saddle point. Contour energies are in MeV.

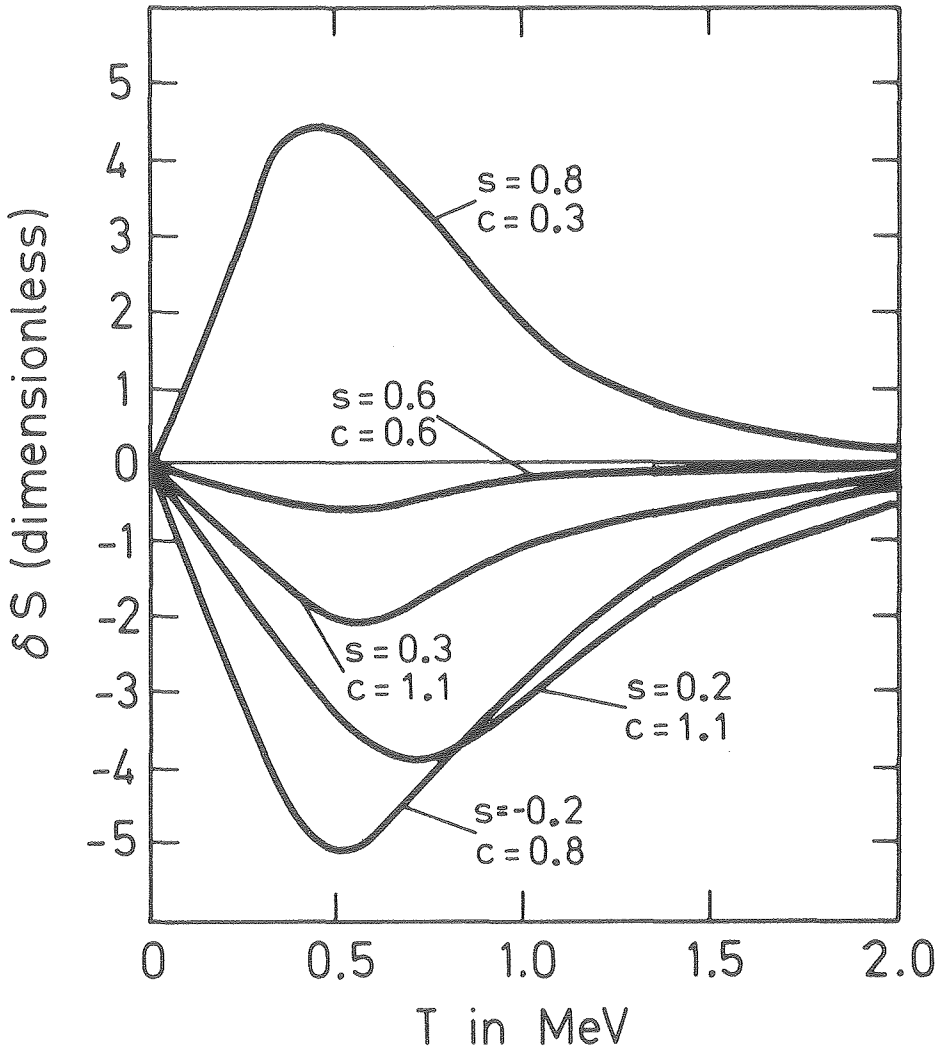

XBL 809-11591

Fig. 6. Shell correction to the entropy versus temperature, $\delta S(def, T)$, for the neutrons of the system $^{292}118$ at various deformations.

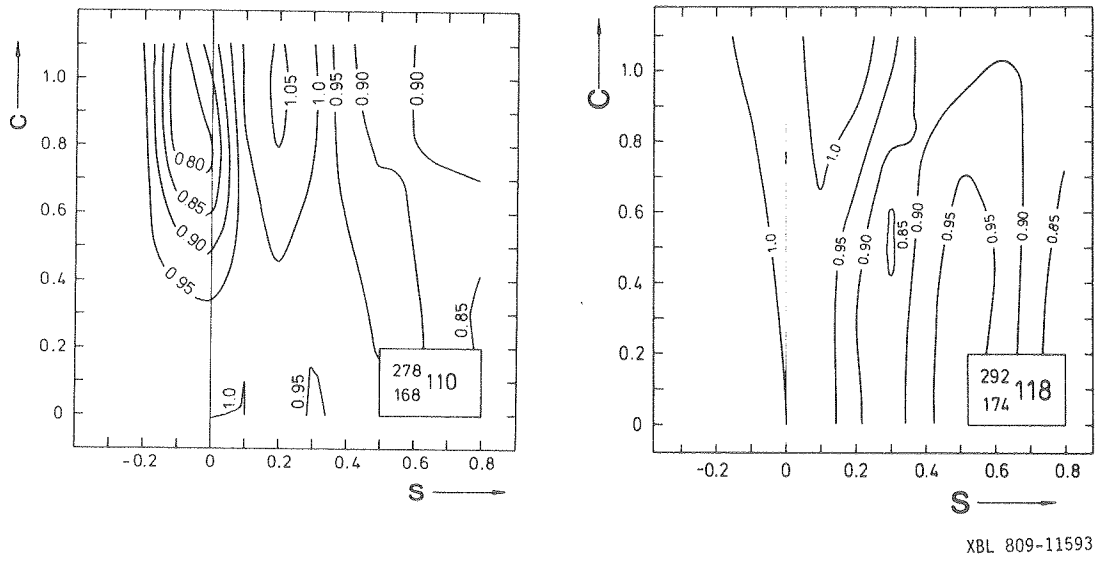

Fig. 8. Contour plots of the temperature in MeV for the isentropic process and the systems indicated. The constant entropy corresponds to a spherical temperature of 1 MeV.

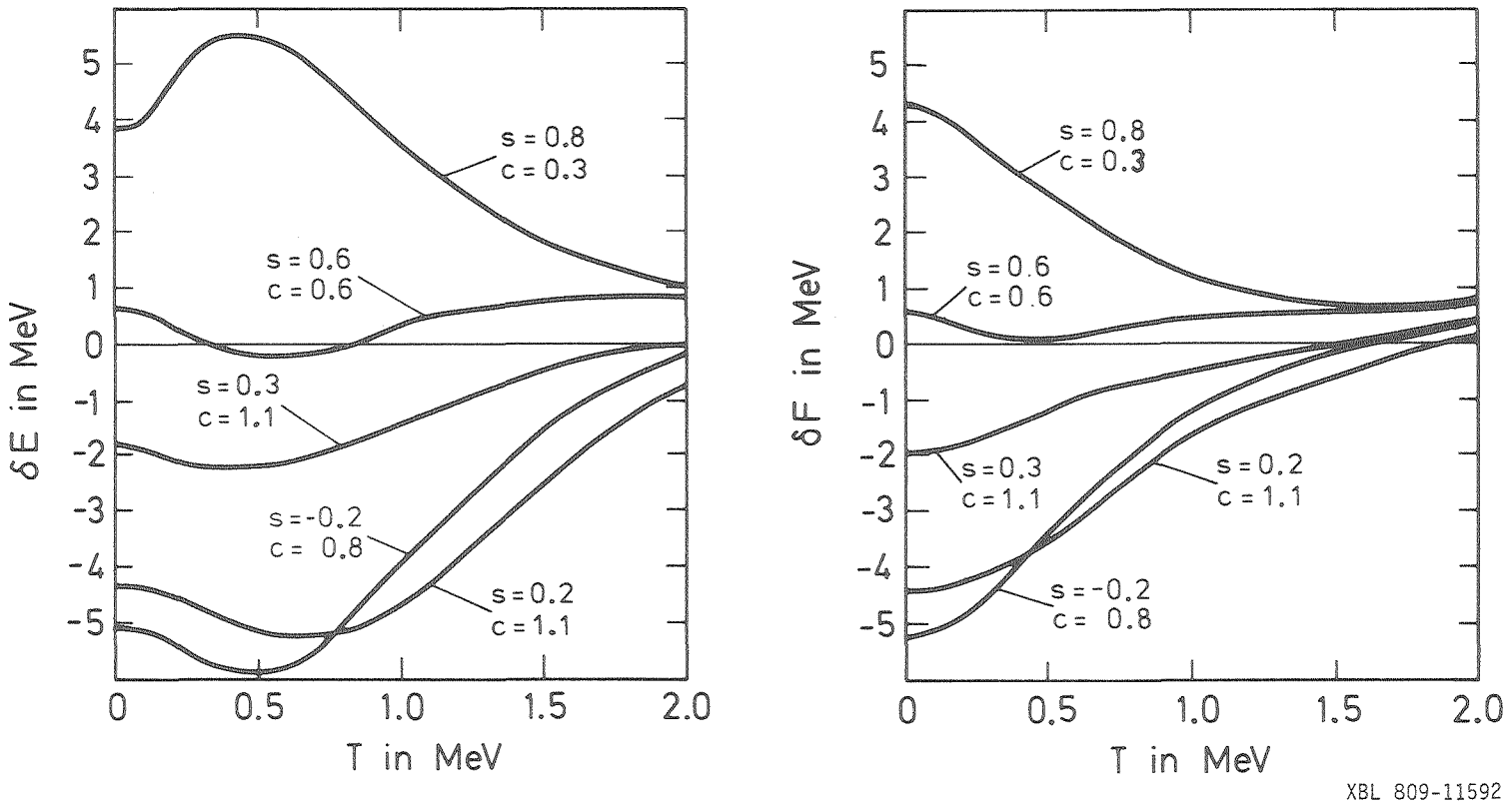

Fig. 7. Shell corrections to the energy (left figure) and to the free energy (right figure) versus temperature for the neutrons of the system $^{292}118$.

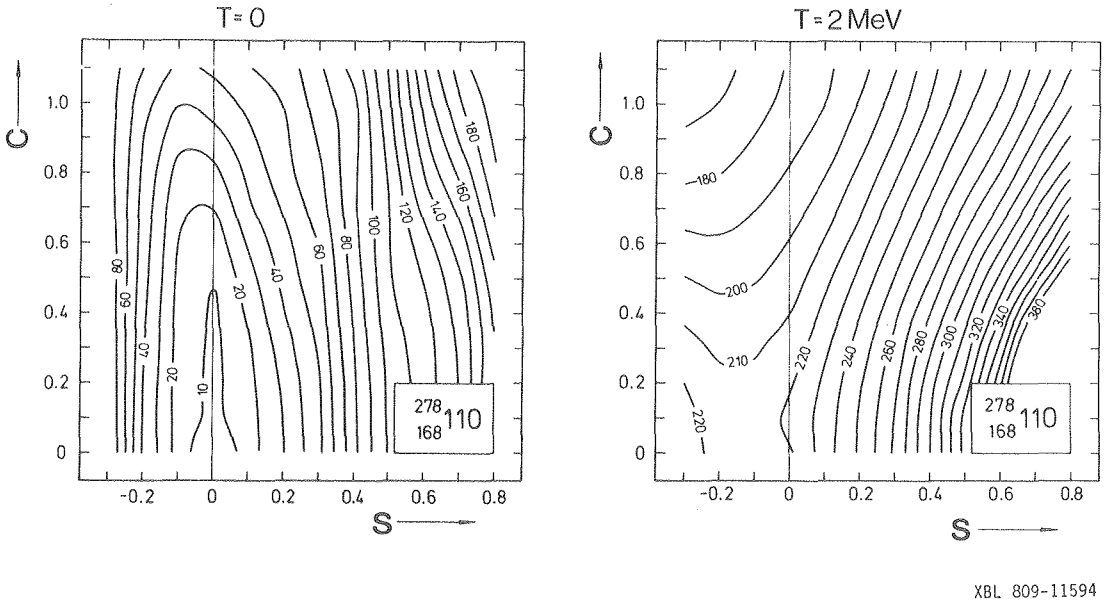

Fig. 9. Contour plot of the perpendicular moment of inertia, $\theta_{\perp}^{CM}(def, T)$ in units of $\hbar^2/MeV$ for $T=0$ (left figure) and $T=2\,MeV$ (right figure) and the system indicated.

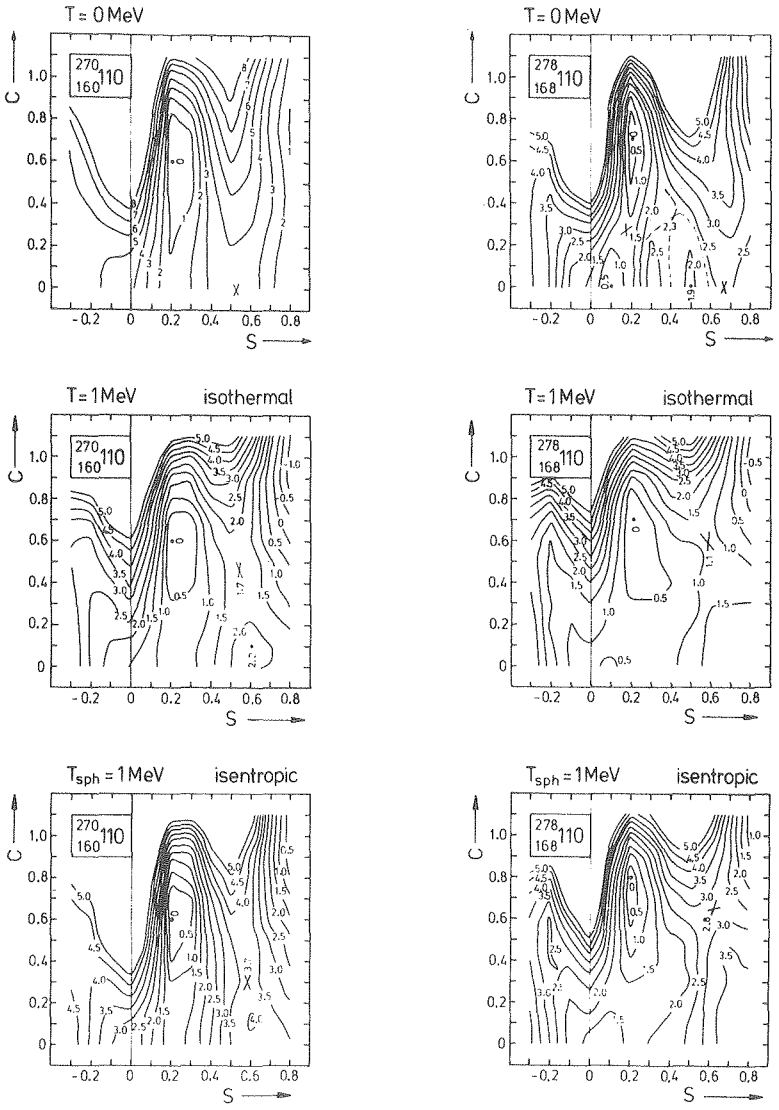

Fig. 10. Contour plots of the free energy (isothermal process) or of the energy (isentropic process) for vanishing angular momentum. For $T=0$ the energy is equal to the free energy.

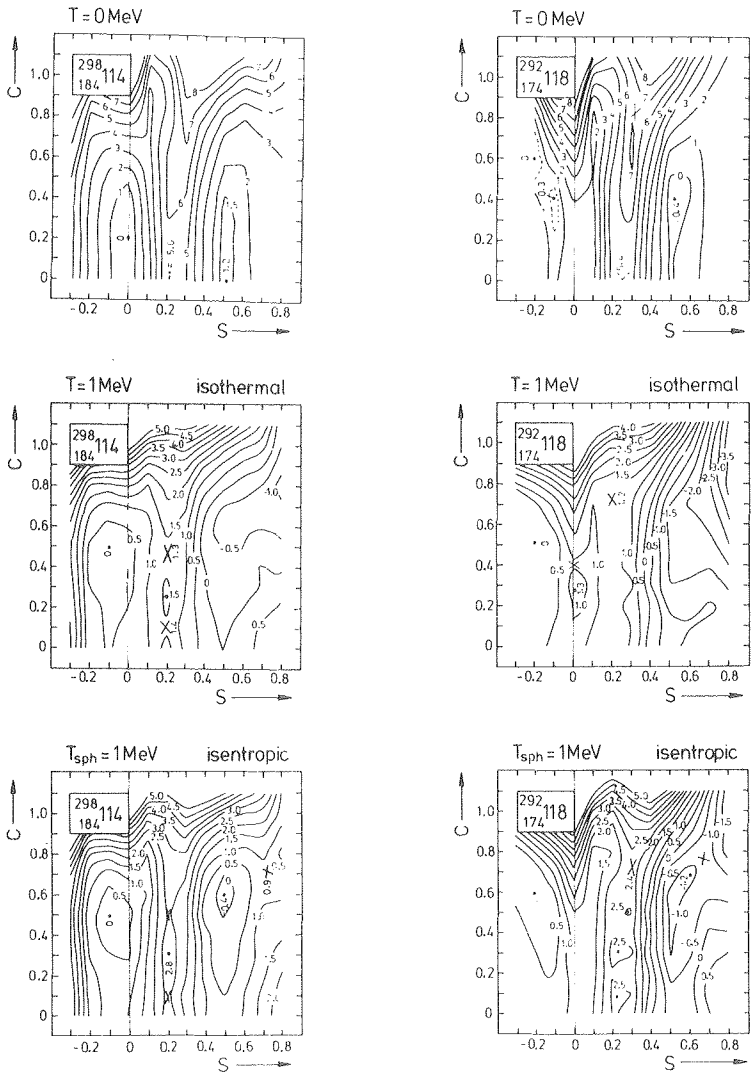

Fig. 11. Same as Fig. 10 but for very heavy systems.

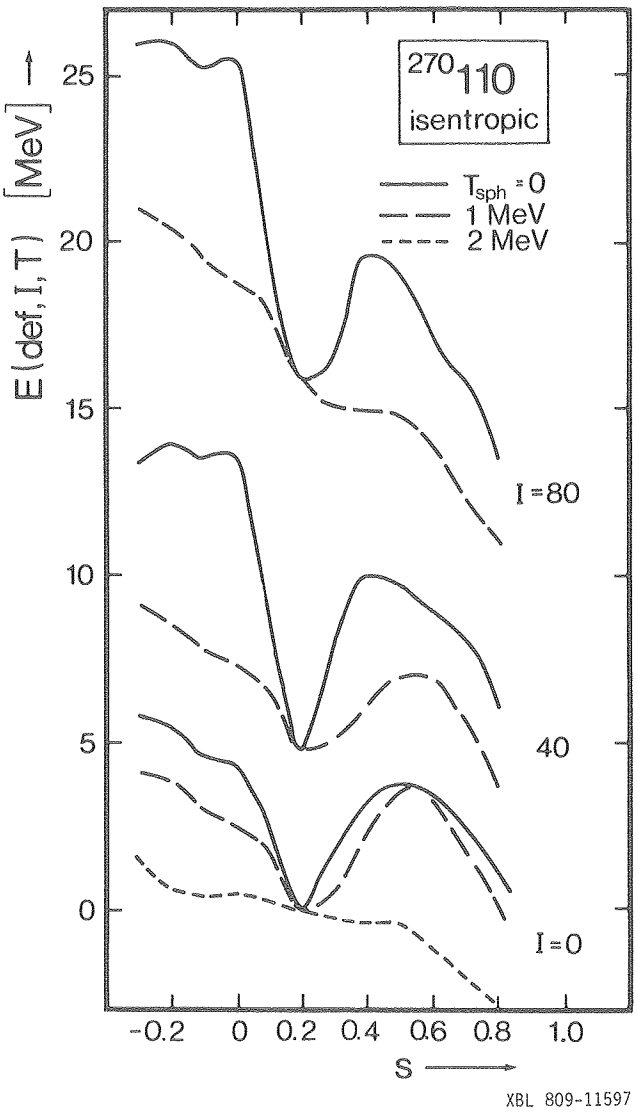

Fig. 12. Deformation energies along the fission path plotted against the elongation deformation coordinate for various angular momenta. Phase transitions through the CAP effect are taken into account.

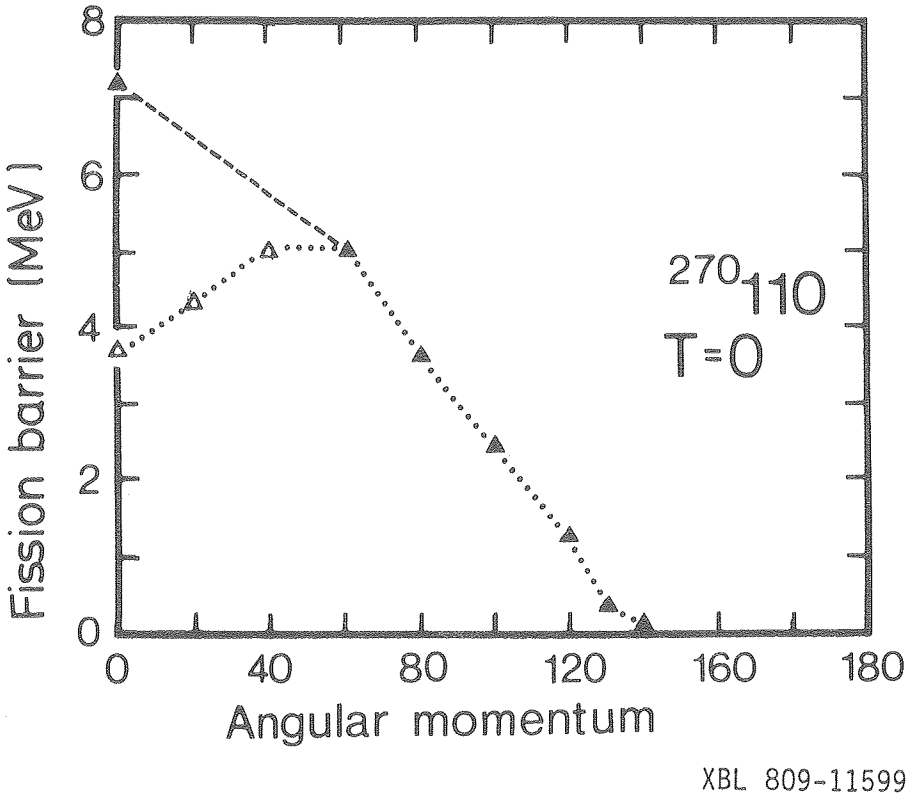

Fig. 13. Dependence of barrier height on angular momentum for the cold system ^{270}110. Open triangles refer to calculations with pairing and full triangles to results without or vanishing pairing.